Journal of Catalysis 284 (2011) 138–147

Contents lists available at SciVerse ScienceDirect

Journal of Catalysis

journal homepage: www.elsevier.com/locate/jcat

Molecular approaches to catalysis
Naked gold nanoparticles as quasi-molecular catalysts for green processes

Mercedes Boronat, Avelino Corma *

Instituto de Tecnología Química, Universidad Politécnica de Valencia – Consejo Superior de Investigaciones Científicas, Av. de los Naranjos, s/n, 46022 Valencia, Spain

ARTICLE INFO

Article history:
Available online 17 October 2011

Keywords:
DFT
Oxidation
Gold species
Reaction mechanism

ABSTRACT

Gold nanoparticles smaller than ~2 nm show interesting catalytic properties arising from their size-determined electronic and geometrical structures. They are able to dissociate molecular O_2 with low activation barriers and become oxidized in a reversible way at low temperature. Several oxygen species adsorbed on the nanoparticle surface, as well as different gold sites including low coordinated neutral Au^0 atoms and cationic Au^I and $Au^{\delta+}$ species, are generated on the oxidized nanoparticles. The implication of these new sites in the mechanism of different gold-catalyzed reactions in which oxygen plays a crucial role is discussed here.

1. Introduction

The current trend toward sustainable development implies the design of new and more efficient chemical processes that minimize the generation of byproducts and the consumption of energy and raw materials. To achieve this, stoichiometric reactions should be replaced by heterogeneously catalyzed processes, able to selectively produce the desired molecules while working under mild reaction conditions. In the search for green processes, selective hydrogenations with molecular H_2 and oxidations with molecular O_2 and carbon–carbon bond forming reactions are among the most pursued objectives. The finding that small gold nanoparticles dispersed on metal oxides are highly active catalysts for CO oxidation with O_2 at low temperature [1] opened a field in heterogeneous catalysis, and the amount of information published about this reaction in the last years is impressive. All this research efforts have shown that particle size, shape, and interaction with the support are key parameters determining the catalytic activity of gold [2–16].

From an industrial point of view, and besides CO oxidation, the value of gold is mainly based on its ability to catalyze organic reactions involved in the synthesis of fine chemicals [17,18]. Thus, selective hydrogenations using molecular H_2 [19–23], water gas shift reaction [24–26], carbon–carbon bond forming reactions [27–33], and oxidation of organic compounds with molecular O_2 [34–36] are catalyzed by gold nanoparticles supported on different carriers at atmospheric pressure and mild reaction temperature. One of the most interesting features of gold catalysts is their high selectivity that allows discriminating between different groups or positions within one molecule. Thus, the nitro group is selectively hydrogenated on Au/TiO_2 and Au/Fe_2O_3 in molecules containing C=C, C=O, or C≡N groups [22], the carbonyl group in α,β-unsaturated aldehydes is selectively hydrogenated over Au/ZrO_2 or Au/ZnO [19,37,38] catalysts, and unsaturated alcohols can be selectively oxidized to unsaturated aldehydes over Au/SiO_2 [35,39].

When dealing with oxidation reactions, one of the most important issues to be considered is O_2 activation and/or dissociation. There are many experimental and theoretical studies showing the key role played by the metal oxide or hydroxide support [40,41] and by special Au sites at the metal–support interface [12,14,42,43] to activate molecular O_2. However, there is also evidence that gold nanoparticles supported on inert materials are able to catalyze a number of oxidation reactions, and in this case, it is particle size the factor determining catalyst activity. Thus, Turner et al. [44] showed that very small gold entities of ~1.5 nm supported on boron nitride, silicon dioxide, or carbon are efficient catalysts for styrene epoxidation with molecular O_2, while particles larger than 2 nm are completely inactive. Haruta et al. [45] reported that, for propene epoxidation with O_2 and H_2 over Au/TS-1 catalysts, Au nanoparticles with diameter between 1 and 2 nm are more active than tiny clusters incorporated inside the micro porous channels. Gold nanoparticles smaller than 2 nm deposited on cellulose [46] or stabilized by poly(N-vinyl-2-pyrrolidone) [47–49] show good catalytic performance in the aerobic oxidation of alcohols, and a recent study on the aerobic oxidation of cyclohexane on a series of size-controlled gold clusters on hydroxyapatite gave an optimum cluster size of 39 atoms, that is ~1 nm [50]. Even in the homocoupling of phenylboronic acid to produce biphenyl catalyzed by small gold nanoparticles (<2 nm) stabilized by poly(N-vinyl-2-pyrrolidone) [27], molecular oxygen dissolved in water was found to be necessary for the reaction to proceed, though it is not an oxidation reaction.

* Corresponding author. Fax: +34 96 387 7809.
E-mail address: acorma@itq.upv.es (A. Corma).

0021-9517/$ - see front matter © 2011 Elsevier Inc. All rights reserved.
doi:10.1016/j.jcat.2011.09.010

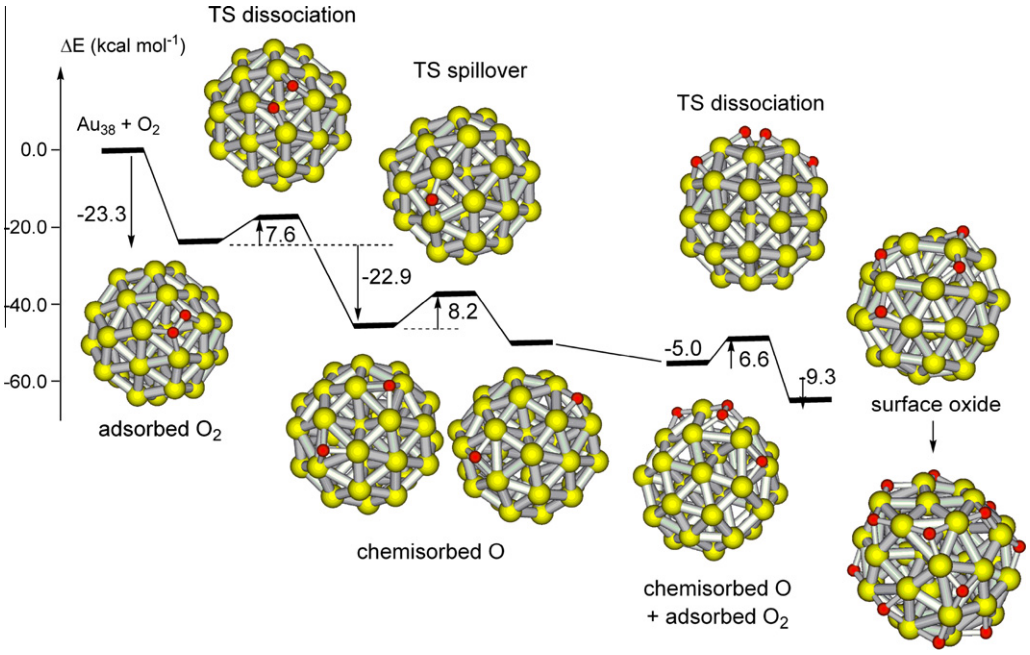

Fig. 1. Calculated energy profile for O_2 dissociation and O spillover on a clean Au_{38} and a partially O-covered $Au_{38}O_2$ nanoparticle.

It appears then that a direct and active participation of the metal oxide support or the gold–support interface in the activation of molecular O_2 is not absolutely mandatory and that there must exist a mechanism for O_2 activation that directly occurs on really small gold nanoparticles. Theoretical studies have shown that this is indeed the case. As clearly explained by Metiu et al. [51], O_2 does not bind to flat gold surfaces but only to rough centers, that is, gold atoms at corners, edges, steps, kinks, etc. The reason is that in clusters and rough surfaces, the highest occupied molecular orbital of gold is localized and its charge density sticks out in the vacuum, facilitating electron density transfer into the π^* orbital of O_2 and inducing the binding of O_2 to gold. It has also been shown on the basis of DFT calculations that strong adsorption of molecular O_2 on isolated gold nanoparticles having low coordinated atoms is a necessary but not sufficient condition for O_2 dissociation [52], and it has been proposed that there is a critical size for gold nanoparticles (~1 nm) to dissociate molecular O_2 [52,53]. But besides particle size, O_2 dissociation is also very sensitive to the arrangement of gold surface atoms. When molecular O_2 adsorbs on a (100) facet of a gold nanoparticle adopting a bridge-bridge conformation (see Fig. 1), the degree of electron density transfer from gold to the π^* molecular orbital of O_2 is larger than in any other conformation [53], so that the O–O bond weakens and dissociation is favored.

Based on the findings described above, we have recently synthesized small gold nanoparticles within a very narrow size distribution (1.1 ± 0.5 nm) on functionalized multiwalled carbon nanotubes [54] and investigated their ability to dissociate molecular O_2. We observed that the surface of gold nanoparticles with diameter between 0.9 and 1.7 nm becomes oxidized in a reversible way at low temperature in the presence of O_2 and that the oxygen atoms from the oxide over layer are highly reactive toward CO to form CO_2 and in the epoxidation of styrene. However, none of these processes was observed on particles with diameter larger than ~4 nm, in agreement with the several examples reported above [44–47,49,50].

It is also known from previous surface science studies that the presence of oxygen atoms on gold surfaces modifies the chemical behavior of gold [55,56], but the nature of the new sites generated and their implication in the mechanism of different gold-catalyzed reactions are not fully understood yet. In the last years, theoretical modeling studies have become a powerful tool providing information about fundamental aspects of catalysis, such as identification of active sites in heterogeneous catalysts and determination of reaction mechanisms. A detailed knowledge of the mode of adsorption and activation of reactants and reaction intermediates, of the energy barriers that have to be overcome, and of the nature of the active sites involved in each elementary step of the overall process, including the desired reaction and the competing routs leading to byproducts, is necessary to design highly selective catalysts. The objective of this article is to analyze, from a theoretical point of view, the nature of the active sites generated on small unsupported gold nanoparticles as a function of oxygen coverage, and to establish their role in some reactions of fundamental and industrial interest: alcohol oxidation, olefin epoxidation, and homocoupling of phenylboronic acid yielding biphenyl. The common feature of these apparently different reactions is that they are catalyzed by gold nanoparticles smaller than 2 nm in the presence of molecular O_2, suggesting that similar active species might be involved.

2. Oxygen dissociation and recombination

The small gold nanoparticles that have been reported to be active in a number of oxidation reactions were modeled by means of an Au_{38} cluster with a typical cuboctahedral shape and ~1 nm diameter. Previous theoretical studies have shown that gold nanoparticles containing from 25 to 79 atoms and with particle diameter around 1 nm can dissociate one O_2 molecule into two separated O atoms with low activation barriers [8,52,53], following the reaction path depicted in Fig. 1. In a first step, molecular O_2 adsorbs in a bridge-bridge conformation on a (100) facet of a clean Au_{38} nanoparticle. This adsorption mode results in a large degree of electron density transfer from gold to the π^* molecular orbitals of O_2, which weakens the O–O bond and facilitates its dissociation, as previously described [53]. The calculated activation energy is only 7.6 kcal/mol, and the process is highly exothermic. After dissociation, the two adsorbed oxygen atoms are placed in separated 3-fold

hollow positions, coordinated to three gold atoms with calculated Au-O distances between 2.15 and 2.20 Å. The energy barrier for spillover to other 3-fold hollow positions is also low, 8.2 kcal/mol, and therefore it can be assumed that oxygen atoms move easily over the particle surface. But the most remarkable aspect of this path is that, after dissociation of the first O_2 molecule, the active site consisting of four gold atoms arranged as in the (100) facet is not occupied by any O atom, so that a second O_2 molecule can adsorb there, be activated through electron density transfer to the π^* molecular orbitals and dissociate with a low activation energy, 6.6 kcal/mol (see Fig. 1). Assuming a cuboctahedral shape for the gold nanoparticles of ~1 nm diameter, and taking into account that there are six active sites on each Au_{38} nanoparticle and that each of these sites can dissociate at least two O_2 molecules with low activation barriers, it seems that it is possible and easy to reach a coverage of one monolayer oxide ($Au_{38}O_{16}$) and even more ($Au_{38}O_{24}$).

Density functional theory studies of oxygen adsorption on the Au(111) surface predicted the formation of a very thin surface-oxide-like structure that would be stable up to temperatures of around 420 K at atmospheric pressure [57,58]. The gold atoms in this oxide layer would be linearly coordinated to two oxygen atoms, in AuO_2 units that would form chains of alternating oxygen and gold atoms. This oxide-like structure was identified by high-resolution electron energy loss spectroscopy [58], together with a less stable chemisorbed oxygen species characterized by oxygen atoms placed on the gold surface and directly coordinated to three gold atoms. These two oxygen species, chemisorbed and oxide-like, are also formed on the Au_{38} cluster considered in this study. As described above, the two oxygen atoms generated by dissociation of a O_2 molecule on the naked Au_{38} cluster are chemisorbed oxygen species, coordinated to three gold atoms with calculated Au–O distances between 2.15 and 2.20 Å. The net atomic charge on these chemisorbed oxygens is −0.8 e, while the gold atoms in direct contact with oxygens become positively charged by ~0.2 e, that is, they become $Au^{\delta+}$ species. After dissociation of a second O_2 molecule at the same site, the four oxygen atoms are arranged in such a way that each gold atom is directly bonded to two oxygen atoms with a linear O–Au–O geometry similar to that found in Au^I complexes. The O–Au–O optimized bond lengths (~2.05 Å) are slightly shorter than the other Au–O distances (between 2.10 and 2.25 Å), and the gold atom involved in the linear structure is slightly shifted upwards with respect to the particle surface. The negative charge on the oxide oxygen atoms is also −0.8 e, but the positive charge on the shared gold atom increases to 0.5 e, indicating that it could be described as Au^I, while that on the gold atoms only bonded to one oxygen is between 0.20 and 0.25 e, suggesting these are $Au^{\delta+}$ species. The same geometrical arrangement and charge distribution is obtained on the $Au_{38}O_{16}$ model depicted in Fig. 1, in which all oxygen atoms are forming the most stable O–Au–O linear structures. Considering that 32 out of the 38 gold atoms of the cluster are on the surface, this model describes a gold nanoparticle covered by a monolayer of gold oxide and contains both Au^I and $Au^{\delta+}$ species.

The energy profile depicted in Fig. 1 provides information not only in relation to O_2 dissociation but also about the reverse process, the recombination of two O atoms yielding molecular O_2. All the intrinsic activation barriers involved in the direct dissociation process are lower than 8.2 kcal/mol. However, since dissociation is exothermic, the intrinsic activation barriers for recombination are higher, and the calculated values depend on oxygen coverage. Thus, the activation energy necessary to form a O_2 molecule from two oxygen atoms adsorbed on a clean Au_{38} nanoparticle is larger than 30 kcal/mol but decreases to 16 kcal/mol when the nanoparticle is partially covered by a surface gold-oxide layer. Isotopic $^{16}O_2/^{18}O_2$ exchange experiments [54] confirmed that O_2 dissociation on gold nanoparticles of 1.1 nm diameter occurs at room temperature, while $^{16}O^{18}O$ release requires more energy and is not observed at temperatures below 80 °C (see Fig. 2). We will now discuss the role that the different oxygen and gold species existing on the gold nanoclusters can play during oxidation reactions.

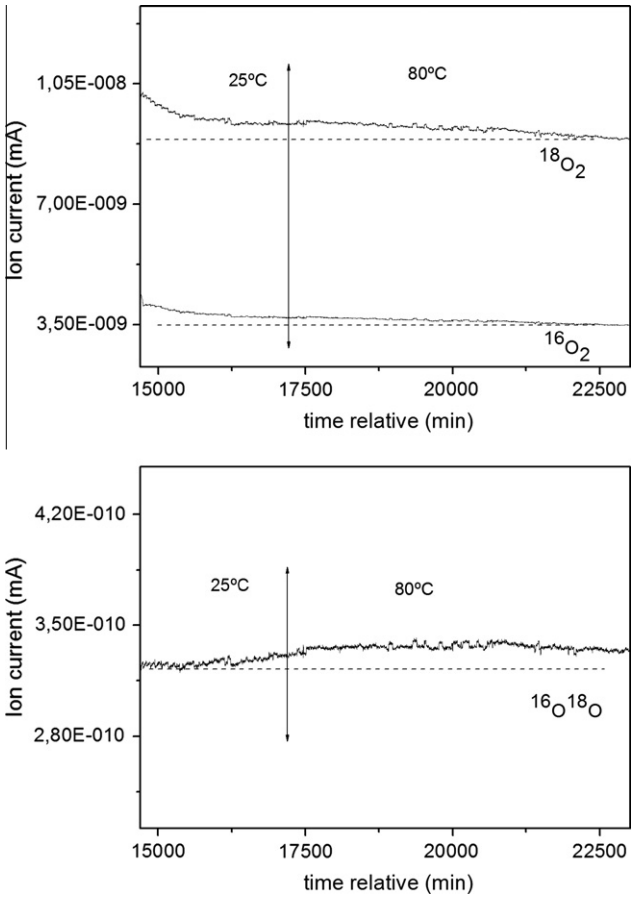

Fig. 2. Isotopic $^{16}O_2/^{18}O_2$ exchange at 25 and 80 °C on gold nanoparticles of 1.1. nm diameter. From Ref. [50].

3. Alcohol oxidation

The selective oxidation of alcohols to aldehydes or ketones is an important step in the synthesis of fine chemicals [59,60], and in recent years, an intense effort has been done to find gold heterogeneous catalysts able to perform alcohol oxidation with molecular O_2 and generating H_2O as the only byproduct [34,35,46–49]. Different studies agree that the complete mechanism for alcohol oxidation involves formation of a metal–alkoxide species that, in a second step, suffers a β-hydride elimination yielding the carbonylic product and a metal–hydride intermediate [59–62]. We recently investigated the mechanism of ethanol oxidation to ethanal on different gold surfaces and on an Au_{38} nanoparticle in the absence of O_2 [63], and found an inverse correlation between the reactivity of the surface and the coordination number of the gold atoms. The most favorable energy profile was obtained on the naked Au_{38} cluster and is depicted in Fig. 3, top. Ethanol adsorbs with the O atom on top of a corner Au atom at a distance of 2.45 Å, releasing 9.0 kcal/mol. In the transition state for the first elementary step, $TS1_{Au}$, the O–H bond is broken and the hydrogen atom of the hydroxyl group and the resulting ethoxy fragment bind to different

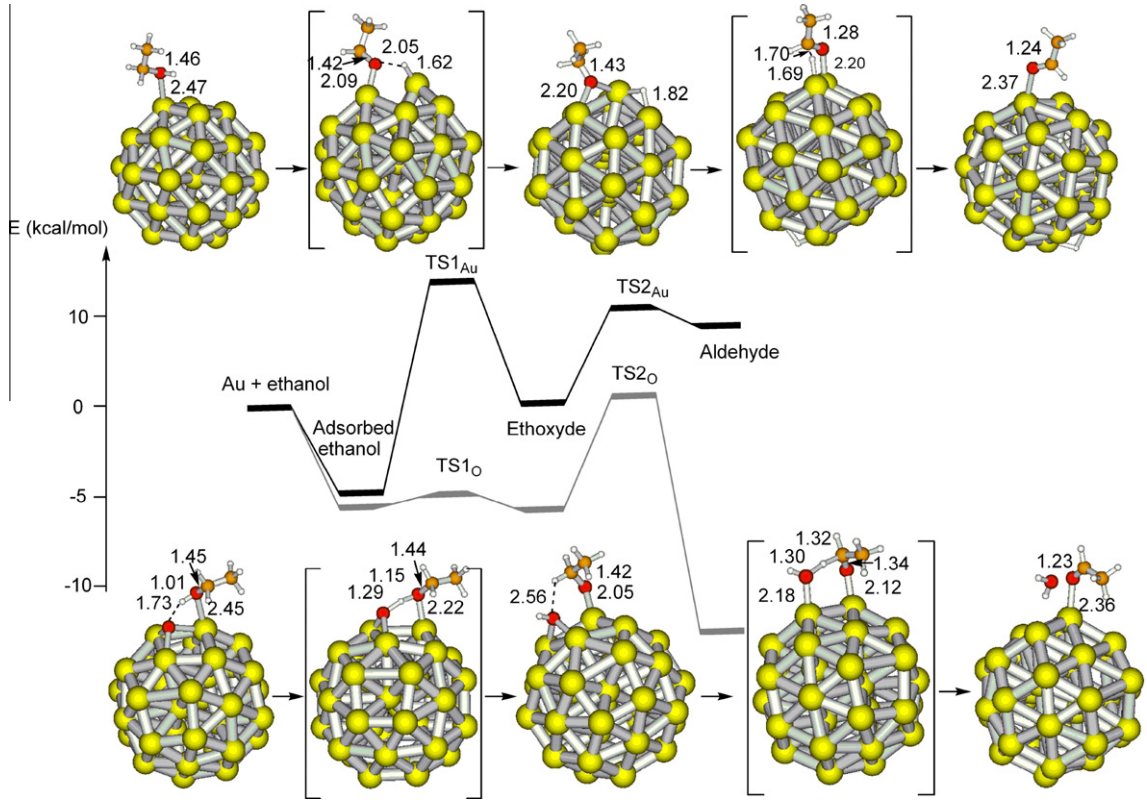

Fig. 3. Calculated energy profile and optimized structures involved in the oxidation of ethanol on a naked Au_{38} nanoparticle (top, black line) and on a Au $_{38}$ nanoparticle with a chemisorbed oxygen atom (bottom, gray line). The most relevant optimized distances are given in Å.

gold sites on the particle surface. In a second step, the C–H_β bond dissociates and the hydrogen atom is transferred to the gold surface, with a calculated activation barrier of 12.0 kcal/mol, yielding adsorbed ethanal. According to this pathway, the rate determining step is the deprotonation of the hydroxyl group, with a calculated activation energy of 24.0 kcal/mol. However, this model does not consider the possibility of alkoxy formation on the metal oxide support and is only valid in absolutely anaerobic conditions, which is not the most usual situation. Therefore, we report now the mechanism of ethanol oxidation to ethanal on gold clusters containing either chemisorbed oxygen species (Fig. 3, bottom) or surface-oxide-like species (Fig. 4) and analyze their role in the kinetics of the reaction.

The presence of a chemisorbed oxygen atom generates slightly positive $Au^{\delta+}$ sites (~0.2 e). Ethanol adsorbs at this sites as strongly as on neutral low coordinated Au^0 sites (see Fig. 3), and a hydrogen bond is formed between the proton of the hydroxyl group and the chemisorbed oxygen atom. This interaction and the configuration of adsorbed ethanol facilitates its deprotonation via transition state $TS1_O$, in which the hydrogen of the hydroxyl group is transferred from one oxygen atom to another in an almost barrier less process. The resulting ethoxy fragment does not occupy a bridge position between two gold atoms as it was found on the clean Au_{38} cluster but is directly attached to a corner gold atom, with the H_β atom oriented toward the surface hydroxyl group. Dissociation of the C–H_β bond and transfer of the H_β atom to the surface hydroxyl requires an activation energy of 13.4 kcal/mol, equivalent to that calculated for the same step on the clean Au_{38} cluster. These results indicate that the presence of chemisorbed oxygen atoms on the gold nanoparticles has a strong influence on the first step of the mechanism, decreasing the activation energy for deprotonation of the alcohol hydroxyl group by 23 kcal/mol but does not facilitate the dissociation of the C–H_β bond; this step becoming the rate determining step of the whole process. A similar trend has been recently reported by Davis et al. in the oxidation of ethanol at high pH [64]. Kinetic measurements and DFT calculations showed that the activation of the alcohol O–H bond is greatly facilitated by the presence of hydroxide species bound to the gold surface, while the effect on the barrier for C–H bond dissociation is much less.

The presence of an oxide-like unit on the gold nanoparticle modifies the energy profile in a different way as chemisorbed oxygen does, as depicted in Fig. 4. Ethanol does not adsorb on the Au^I atom linked to two oxygen atoms, bearing a net charge of 0.5 e, but on the $Au^{\delta+}$ species only bonded to one oxygen atom, that is positively charged by only 0.2 e. Although the geometry of the adsorbed ethanol structure is equivalent to that obtained for the previously presented model with chemisorbed oxygen, the process is not energetically favored on the oxide-like surface, and the calculated adsorption energy is slightly positive. It should be remarked at this point that, in all these studies, the positions of most of the gold atoms of the Au_{38} cluster are kept fixed, and only the C, H, O, and the Au atoms directly bonded to oxygens are allowed to relax. A larger degree of geometry relaxation could modify the energy profile and might turn ethanol adsorption into slightly exothermic, but not as much as it was found with the other two considered models. One can also assume a Eley–Rideal mechanism in which the reactant from the gas phase is converted into the ethoxide intermediate through transition state $TS1_{ox}$ without the need of being previously adsorbed on the particle. The calculated activation energy for this step is low, 4.2 kcal/mol, and the reaction is slightly endothermic. Again, it is possible that a larger degree of geometry relaxation could stabilize the ethoxide intermediate in relation to $TS1_{ox}$, but not enough to change the conclusion that the presence of oxide-like oxygens does not favor ethoxide coordination to the gold nanoparticle. The species that is directly obtained from ethanol deprotonation via $TS1_{ox}$ is the

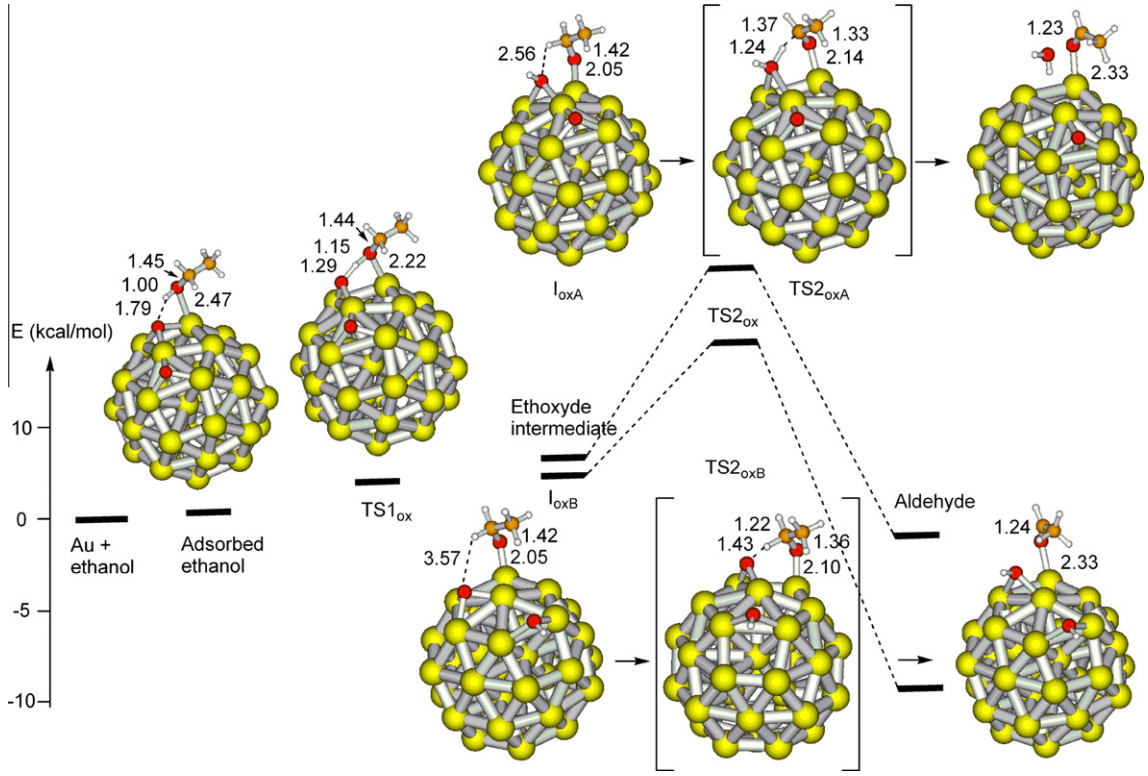

Fig. 4. Calculated energy profile and optimized structures involved in the oxidation of ethanol on a partially oxidized Au_{38} nanoparticle. The most relevant optimized distances are given in Å.

ethoxide intermediate I_{oxA} depicted in Fig. 4, top. The ethoxide fragment is directly attached to a corner gold atom bearing a positive charge of 0.26 e, and the net atomic charge on the gold atom in the oxide-like unit is 0.39, indicative of a Au^{I} species. A second ethoxide intermediate has been considered, I_{oxB} in Fig. 4, bottom, in which the proton abstracted from ethanol in the first reaction step is attached to the oxygen atom further from the ethoxide fragment. In this structure, which is 1.8 kcal/mol more stable than I_{oxA}, the AuO_2 unit has decomposed into a chemisorbed oxygen and a hydroxyl group, and the net atomic charge on the "Au^{I}" species decreases to 0.26 e, because it is now only directly bonded to one oxygen atom. Therefore, only Au^0 and $Au^{\delta+}$ species are present on I_{oxB}. To check whether this difference in charge distribution plays a role in the reactivity of the system, the transition states for the C–H_β bond scission step were calculated starting from both ethoxide intermediates (see Fig. 4), and the conclusion is that the presence of cationic Au^{I} species has a clear negative effect on the activity of gold nanoparticles toward alcohol oxidation. The calculated activation energy for the transfer of H_β to a chemisorbed oxygen atom through transition state $TS2_{oxB}$ is 13.2 kcal/mol, similar to the values obtained on the clean Au_{38} nanoparticle and on the model containing chemisorbed oxygen. However, the calculated barrier for the reaction occurring through transition state $TS2_{oxA}$ is considerably higher, 20.4 kcal/mol. This is not due to the nature of the group to which H_β is being transferred, a surface hydroxyl group instead of an oxygen atom, but to the stronger interaction of the hydroxyl group in I_{oxA} as compared to I_O. In this last case, the surface hydroxyl group was bonded to two $Au^{\delta+}$ species, and it was not difficult to break one of these interactions to form a H_2O molecule. In the I_{oxA} intermediate, however, the surface hydroxyl group is directly attached to a cationic Au^{I} atom, and a higher energy is required to break this strong bond.

The conclusion from these theoretical results is that while the presence of chemisorbed oxygen atoms on the gold surface facilitates considerably the first OH deprotonation step without modifying the good performance of the catalyst in the second step, the presence of a surface-oxide-like monolayer has a clear negative impact on the activity of gold nanoparticles toward alcohol oxidation, and its formation should be avoided.

In this sense, recent work from Tsukuda et al. has shown that gold clusters smaller than 1.5 nm and negatively charged by electron donation from the PVP stabilizer are active in benzylic alcohol oxidation under basic conditions [47,48] and that the rate determining step of the process is the dissociation of the C–H_β bond. A mechanism was proposed according to which the H_β atom is abstracted from the alcohol by peroxo- or superoxo-O_2 species adsorbed on gold, although no experimental evidence for the formation of peroxo- or superoxo-species was obtained by ESR or IR spectroscopy [48]. However, the results obtained by Tsukuda et al. are consistent with the mechanism described here in where chemisorbed oxygen atoms generated by dissociation of adsorbed O_2 on really small gold nanoparticles with low activation barriers are the active species in alcohol oxidation, following the mechanism depicted in Fig. 3, bottom. Since a crucial aspect of this mechanism is the need to avoid formation of an oxide-like monolayer on the surface of the gold nanoparticles, further work is being done in our group to check the influence of oxygen coverage on the activity of the recently synthesized nanoparticles [54] toward alcohol oxidation.

4. Olefin epoxidation

Epoxides are versatile intermediates of great value in synthetic organic chemistry and chemical technology. Ethene epoxide (EO) is industrially produced by the direct silver-catalyzed heterogeneous partial oxidation of ethylene with O_2 [65,66], but propene epoxidation by this route results in a very low selectivity toward the

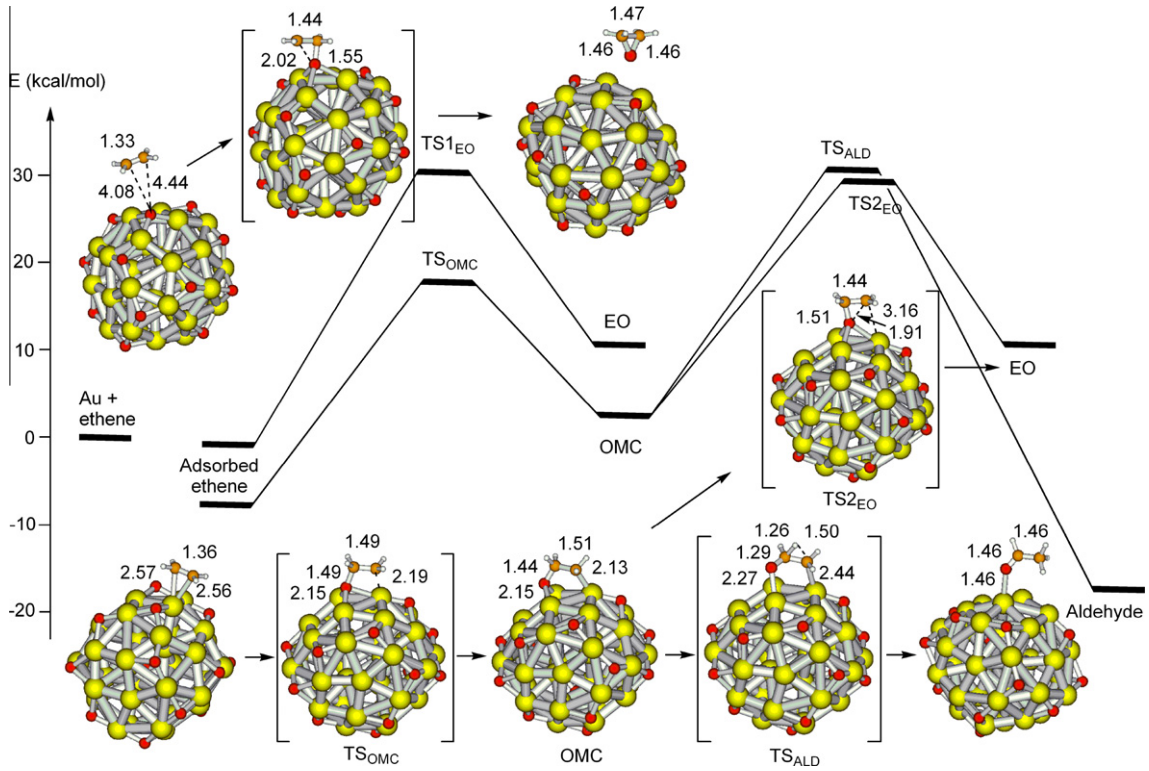

Fig. 5. Calculated energy profile for ethene epoxidation on an oxidized $Au_{38}O_{16}$ nanoparticle. The most relevant optimized distances are given in Å.

epoxide (<50%) [67], and the commercial production of propene oxide (PO) is carried out either by the chlorohydrin process or by the hydroperoxide process, both leading to undesirable by-products [68]. A promising alternative route is based on the direct epoxidation of propene with O_2 and H_2 on Au/TiO_2, $Au/Ti\text{-}SiO_2$ or Au/TS-1 catalysts, generating H_2O as the only byproduct [45,69–73]. In this process, hydrogen peroxide is formed in situ from H_2 and O_2 over the supported gold nanoparticles and reacts with propene over titanium sites [74–76]. A different route involving only gold active sites has been recently reported in the epoxidation of different alkenes [36,44,54]. It has been shown that gold nanoparticles supported on inert materials catalyze styrene epoxidation if their diameter is below 2 nm [44,54], and this seems to be related with the ability of such small gold clusters to dissociate O_2. In fact, styrene epoxidation occurs on Au(1 1 1) surfaces oxidized with ozone at 200 K, a method leading to formation of oxygen-covered gold nanoparticles [77].

We present here the complete reaction path for ethene (Fig. 5) and propene (Fig. 6) epoxidation on the $Au_{38}O_{16}$ model, describing a gold nanoparticle covered by an oxide-like monolayer. The energy profiles are compared with those previously reported for ethene [78,79] and propene [80,81] epoxidation on silver and gold catalysts. The first important aspect to be remarked is that the interaction of the double bond in the olefin with small gold nanoparticles is stronger than with extended gold surfaces [81], and comparable to olefin adsorption on silver surfaces [79]. Ethene adsorbs on a $Au^{\delta+}$ species of the oxide-covered nanoparticle releasing 7.3 kcal/mol, and as a consequence the CC bond length increases by 0.03 Å. Following a mechanism equivalent to that reported for ethene epoxidation on silver surfaces, an oxametalacycle (OMC) intermediate is formed via transition state TS_{OMC}, with a calculated activation barrier of 17.8 kcal/mol. In the OMC structure, the CC bond has evolved from double to single, with an optimized bond length of 1.51 Å; one of the carbon atoms is attached to a surface gold atom at a Au–C distance of 2.13 Å, and the other one is bonded to an oxygen atom with a calculated C–O bond length of 1.44 Å. This geometry is completely equivalent to that previously reported for OMC structures on silver catalysts and is the starting point for two reaction paths leading to formation of the desired EO or the undesired aldehyde. The first process occurs through transition state $TS2_{EO}$ and implies the breakening of the Au–C and Au–O interactions and the formation of a new O–C bond. The second process occurs via transition state TS_{ALD} and involves a 1,2-H shift that converts the OMC intermediate into an aldehyde molecule strongly attached to a gold atom. The calculated activation barriers are similar, ~32 kcal/mol, and about 10 kcal/mol higher than those reported for ethene epoxidation on silver [79]. But the most interesting result from the present study is the finding of a reaction path that directly converts ethene into EO through transition state $TS1_{EO}$, without formation of an OMC intermediate. This path is depicted in Fig. 5, top, and starts with ethene not attached to a surface gold atom but placed above a surface oxygen atom. Although this structure is less stable than that previously described, it might also exist taking into account that the nanoparticles are completely covered by the surface-oxide layer. In the transition state $TS1_{EO}$, the interaction between ethene and the surface oxygen atom causes a lengthening of the CC bond to 1.44 Å, and a weakening of the Au–O bonds, which increase from ~2.2 to ~2.5 Å. The optimized structures of $TS1_{EO}$ and $TS2_{EO}$ are quite similar, the only difference being related to the orientation of the carbon atom not directly attached to oxygen. Thus, while in $TS2_{EO}$, this carbon atom is still oriented toward the gold atom to which it was attached in the OMC intermediate, in $TS1_{EO}$, the carbon atom is pointing out of the particle, with no possibility to form an Au–C bond. To check that these two similar transition states were really involved in two different reaction pathways, we performed the pertinent frequency calculations and four new geometry optimizations which, starting from the optimized structures of $TS1_{EO}$ and $TS2_{EO}$, searched for the corresponding minima. These calculations confirmed the results described above and show that there is a reaction pathway for

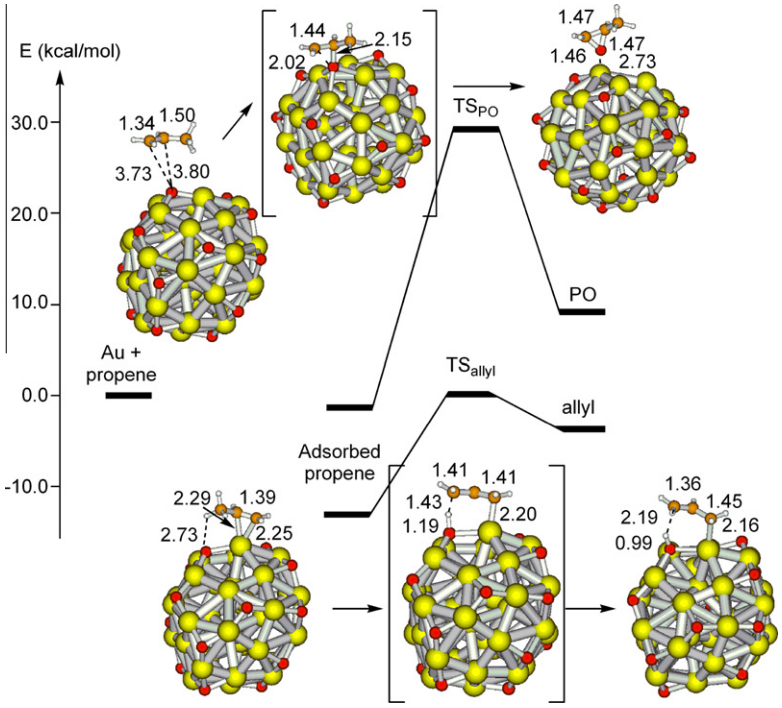

Fig. 6. Calculated energy profile for propene epoxidation (top) and formation of an allyl intermediate (bottom) on an oxidized $Au_{38}O_{16}$ nanoparticle. The most relevant optimized distances are given in Å.

the direct epoxidation of ethene by oxidized gold nanoparticles that involves an activation barrier not higher than that obtained for the classical mechanism via an oxametalacycle intermediate.

However, the silver-catalyzed ethene epoxidation is highly efficient, and the challenge is to find a heterogeneously catalyzed process for propene epoxidation with molecular O_2. The low selectivities to PO obtained using silver catalysts are related to the high reactivity of the hydrogen atoms of the propene methyl group, that are easily abstracted by surface oxygen atoms yielding an allylic intermediate that finally results in total combustion [67,80]. The validity of this mechanism has been indirectly demonstrated by comparing the selectivity to the epoxide of different compounds with (propene, 6%) and without (ethene, 47%, and 3,3-dimethyl-1-butene, 25%) allylic C–H bonds [67,80]. Theoretical studies of propene epoxidation on Ag(1 1 1), Cu(1 1 1), and Au(1 1 1) surfaces indicate that the barrier for OMC formation from co-adsorbed propene and oxygen is ~13 kcal/mol on all surfaces, while the barrier for H abstraction decreases from 14 kcal/mol on Cu(1 1 1) to 7 kcal/mol on Ag(1 1 1) and 5 kcal/mol on Au(1 1 1) [80,81]. These values suggest that gold is not the best candidate to perform the selective epoxidation of propene. However, this conclusion can be wrong if one does not take into account that, as discussed in this manuscript, the catalytic behavior of small gold nanoparticles is different from that of extended surfaces. Moreover, none of the previously mentioned theoretical studies considered the possibility of a one-step pathway for direct olefin epoxidation by surface oxygen atoms such as the one we described above for ethane. Therefore, it is worth to study the above reaction path for the epoxidation of propene on oxidized gold nanoclusters.

As shown in Fig. 6, top, there is a transition state TS_{PO} that directly connects an adsorption complex in which propene is placed above a surface oxygen atom, with a PO molecule weakly interacting with the gold nanoparticle. In this structure, the oxygen atom attacks the central carbon atom of propene, and since there is not any nearby gold atom to interact with the primary carbon atom of the CC double bond, the epoxide is formed. The stability of this adsorbed propene with respect to separated reactants is low, and the activation energy for PO formation is 29.7 kcal/mol, similar to that obtained for direct ethene epoxidation. The competing route leading to formation of a highly reactive allyl intermediate is depicted in Fig. 6, bottom. Propene interaction with a $Au^{\delta+}$ species of the oxide-covered nanoparticle is exothermic by 13.0 kcal/mol, the optimized C–Au distances are ~0.3 Å shorter than those obtained for adsorbed ethene, and the CC double bond length increases to 1.39 Å. In this structure, the methyl group lies close to the gold nanoparticle, with one H atom clearly oriented toward a surface oxygen atom. With this conformation, the abstraction of the H atom by the oxide-like oxygen through transition state TS_{ALLYL} is easy and involves an intrinsic activation energy of 13.9 kcal/mol. Although this value is higher than that reported for allyl formation on a Au(1 1 1) surface [81], it is considerably lower than the barrier obtained for direct propene epoxidation (29.7 kcal/mol) and suggests that oxidized small gold nanoparticles will not be selective catalysts in epoxidation reactions. The apparent contradiction between this conclusion and the recent finding that very small gold clusters supported on inert materials effectively catalyze the epoxidation of styrene by O_2 is not so when the product distribution reported in Refs. [44,54] is analyzed. In both studies, the most abundant product is benzaldehyde, and the amount of styrene epoxide observed is ~5 times lower. A different mechanism in which benzaldehyde is initially formed by oxidative cleavage of styrene and, in a second step, acts as a co reactant in the presence of molecular O_2 according to a peracid and/or acylperoxo radical mechanism has also been proposed [82] and might be occurring in these cases. The conclusion from the present theoretical study is that small gold nanoparticles covered by a surface-oxide layer could be efficient catalysts in the epoxidation of ethene but will probably lead to total combustion in the case of propene.

5. C–C bond forming reactions

Coupling of aryl organic compounds is a powerful and versatile tool in synthetic organic chemistry that allows to obtain biaryls,

which are important building blocks in many natural products and biologically active compounds [83,84]. In particular, the homocoupling of arylboronic acids is catalyzed by gold complexes in homogeneous phase [85,86] and by small gold nanoparticles (<2 nm diameter) either supported on CeO_2 [87] or stabilized by polymers [27,32]. Although this is not an oxidation reaction, it has been shown that the active species in Au/CeO_2 and Au/chitosan are cationic Au(III) atoms stabilized by interactions with the support [85,87]. On the other hand, although cationic gold has not been detected in the gold nanoparticles stabilized by poly(N-vinyl-2-pyrrolidone) in Ref. [27], the presence of molecular O_2 dissolved in water was found to be necessary for the reaction to proceed, suggesting that oxygen species are directly involved in the coupling reaction. Therefore, in this section, we have investigated the mechanism of homocoupling of phenylboronic acid on a naked and a partially oxidized Au_{38} nanoparticle, with the aim of determining which is the role played by cationic gold species and by adsorbed oxygen atoms.

It is generally accepted that phenylboronic acid is activated by a base (usually K_2CO_3 or K_3PO_4) that is always added to the reaction media. The $Ph{-}B(OH)_3^-$ anion generated by interaction of phenylboronic acid with the base adsorbs on the naked and partially oxidized gold nanoparticles forming the C_{Au} and C_{ox} complexes depicted in Fig. 7a. The optimized geometries of both structures are quite similar, with the carbon atom bonded to boron and one of the oxygen atoms of the hydroxyl groups interacting with two gold atoms at the edge of the particle. However, the stability of these two complexes is very different, and while adsorption of $Ph{-}B(OH)_3^-$ anion on the model containing only neutral Au^0 atoms releases 34.3 kcal/mol, its adsorption on cationic $Au^{\delta+}$ sites is exothermic by only 4.7 kcal/mol. This indicates that in catalysts containing both Au^0 and $Au^{\delta+}$ sites, the $Ph{-}B(OH)_3^-$ anion will be preferentially adsorbed and activated on neutral atoms, and therefore, only the complete reaction path for its dissociation on the clean Au_{38} cluster has been calculated. According to this path, $Ph{-}B(OH)_3^-$ anion dissociation occurs through transition state

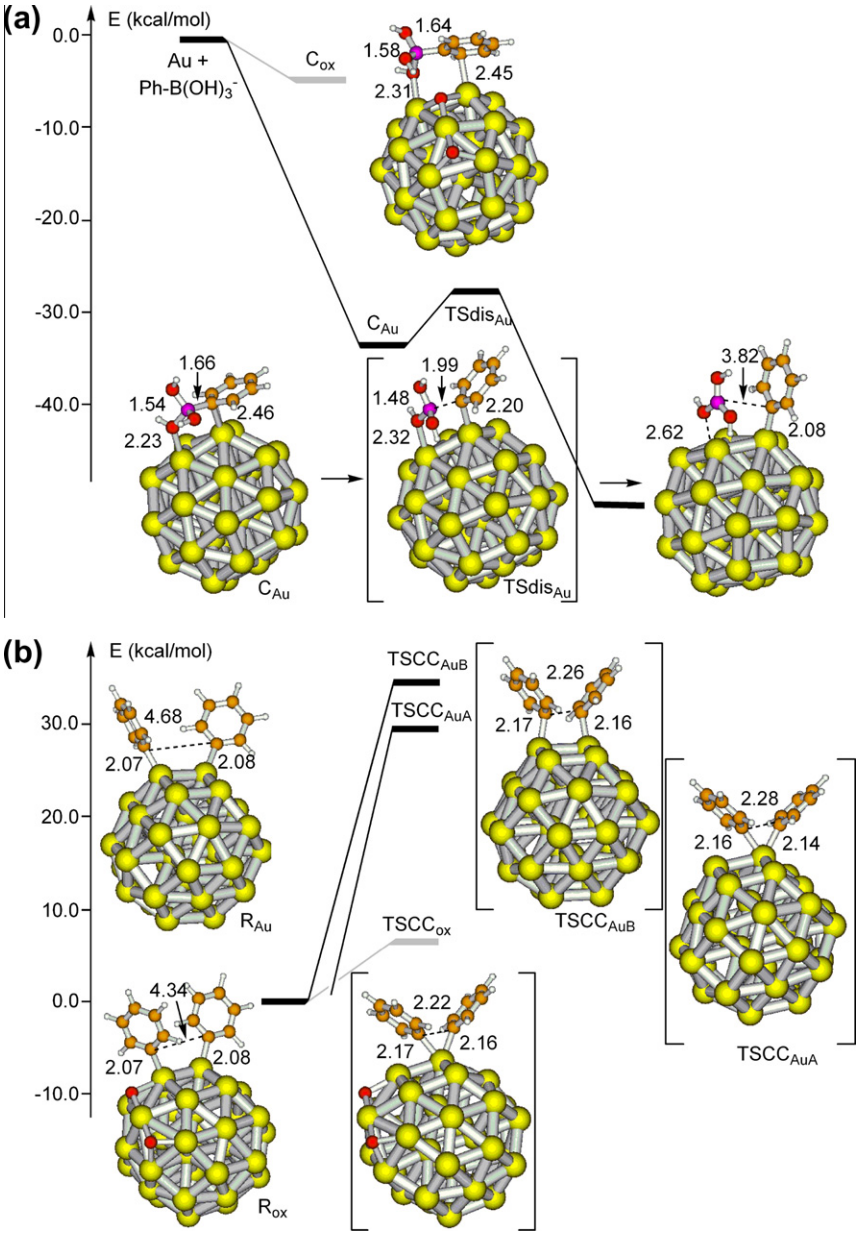

Fig. 7. Calculated energy profile for (a) dissociation of $Ph{-}B(OH)_3^-$ anion and (b) coupling of two phenyl fragments yielding biphenyl on a naked Au_{38} nanoparticle (black line) and on a partially oxidized Au_{38} nanoparticle (gray line). The most relevant optimized distances are given in Å.

$TSdis_{Au}$ (see Fig. 7a) with an activation barrier of only 6.5 kcal/mol, yielding a phenyl fragment strongly attached to a low coordinated gold atom and a molecule of acid boric ($B(OH)_3$) weakly adsorbed on the gold nanoparticle. If this process happens twice, two $B(OH)_3$ molecules will be released, and two phenyl fragments will remain attached to the gold nanoparticle, as in the structure R_{Au} depicted in Fig. 7b. The Au–C bond lengths are short, 2.07–2.08 Å, and the C–C distance is 4.68 Å. From this starting point, two different transition states were localized leading to biphenyl. In $TSCC_{AuA}$, the two phenyl groups are directly attached to the same corner gold atom at ~2.15 Å, and the optimized C–C distance is 2.28 Å. In transition state $TSCC_{AuB}$ each phenyl fragment is bonded to one gold atom, with a geometry more similar to that of the reactant R_{Au} structure. The calculated activation energies through $TSCC_{AuA}$ and $TSCC_{AuB}$ are really high, 30.7 and 35.0 kcal/mol, respectively, suggesting that cationic gold species could play a role in the C–C bond forming step and need to be considered in the theoretical study. The optimized structures of the reactant complex R_{ox} and the transition state for the C–C bond forming step $TSCC_{ox}$ obtained on the partially oxidized gold nanoparticle are similar to those found on the clean Au_{38} cluster, with slightly shorter C–C distances. But the calculated activation energy on the oxidized particle is much lower, only 6.5 kcal/mol, indicating that the crucial role played by dissolved O_2 in the homocoupling of phenylboronic acid catalyzed by gold nanoparticles [27] could be related with the coupling step, and not so much with the activation of phenylboronic acid. It should also be mentioned that the cationic gold species existing in the models used in this work are not Au^{III} atoms, but Au^{I} and $Au^{\delta+}$. The role of Au^{III} sites present in Au/CeO_2 in different coupling reactions is being theoretically and experimentally investigated in our group.

6. Conclusions

Gold nanoparticles smaller than ~2 nm show interesting catalytic properties arising from their size-determined electronic and geometrical structures. They are able to dissociate molecular O_2 with low activation barriers and become oxidized in a reversible way at low temperature. The system is far from simple since it may include several oxygen species adsorbed on the nanoparticle surface, as well as different gold sites including low coordinated neutral Au^0 atoms and cationic Au^{I} and $Au^{\delta+}$ species. In this paper, we have analyzed, from a theoretical point of view, the nature of the active sites generated on small unsupported gold nanoparticles when their surface becomes oxidized by interaction with molecular O_2 and have investigated their role in several gold-catalyzed reactions: alcohol oxidation, olefin epoxidation, and homocoupling of phenylboronic acid yielding biphenyl.

As regards the mechanism of selective alcohol oxidation to aldehyde, it has been found that the presence of chemisorbed oxygen atoms on the gold surface facilitates considerably the first OH deprotonation step to produce the alkoxide intermediate, without modifying the good performance of the catalyst in the second step, the abstraction of the H_β yielding the aldehyde. However, the presence of a surface-oxide-like monolayer has a clear negative impact on the activity of gold nanoparticles toward alcohol oxidation, and its formation should be avoided. In the case of olefin epoxidation, the conclusion from the present study is a bit disappointing: small gold nanoparticles covered by a surface-oxide layer could be efficient catalysts in the epoxidation of ethene, but would probably lead to total combustion of propene. Finally, it has been established that the crucial role played by dissolved O_2 in the homocoupling of phenylboronic acid catalyzed by gold nanoparticles is not related to the activation of phenylboronic acid, but to the coupling step in which the new C–C bond is formed. The present work suggests that the nature of the surface gold atoms on small nanoparticles can be different when in absence or presence of oxygen, and different even with different degree of surface oxygen coverage. At low coverages, dissociated chemisorbed oxygen species exist that also result in formation of $Au^{\delta+}$ species. At full oxygen coverage, when an "oxide layer" is formed on the nanoparticle, Au^{I} species are also formed, and linear O–Au–O bonds cover the surface. It is clear that while the nature of the surface oxygen species will be determinant for many oxidation reactions, the cationic gold species formed because of the surface oxygens will not only be important in oxidation reactions, but also as Lewis acid sites in other non-oxidation reactions.

Acknowledgments

Financial support by the Spanish MICINN (MAT2009-14528-C02-01 and PLE2009-0046) and CONSOLIDER Ingenio 2010-MULTICAT is gratefully acknowledged. We thank *Red Española de Supercomputación* (RES) and *Centre de Càlcul de la Universitat de València* for computational resources and technical assistance.

References

[1] M. Haruta, T. Kobayashi, H. Sano, N. Yamada, Chem. Lett. (1987) 405.
[2] M. Haruta, Catal. Today 36 (1997) 153.
[3] G.C. Bond, D.T. Thomson, Catal. Rev. Sci. Eng. 41 (1999) 319.
[4] M.S. Chen, D.W. Goodman, Acc. Chem. Res. 39 (2006) 739.
[5] G.J. Hutchings, Catal. Today 100 (2005) 55.
[6] S. Carrettin, P. Concepción, A. Corma, J.M. López-Nieto, V.F. Puntes, Angew. Chem. Int. Ed. 43 (2004) 2538.
[7] J. Guzman, S. Carrettin, A. Corma, J. Am. Chem. Soc. 127 (2005) 3286.
[8] N. López, T.V.J. Janssens, B.S. Clausen, Y. Xu, M. Mavrikakis, T. Bligaard, J.K. Nørskov, J. Catal. 223 (2004) 232.
[9] T.V.J. Janssens, B.S. Clausen, B. Hvolbæk, H. Falsig, C.H. Christensen, T. Bligaard, J.K. Nørskov, Top. Catal. 44 (2007) 15.
[10] N. Weiher, A.M. Beesley, N. Tsapatsaris, L. Delannoy, C. Louis, J.A. van Bokhoven, S.L.M. Schroeder, J. Am. Chem. Soc. 129 (2007) 2240.
[11] R. Coquet, K.L. Howard, D.J. Willock, Chem. Soc. Rev. 37 (2008) 2046.
[12] A.A. Herzing, C.J. Kiely, A.F. Carley, P. Landon, G.J. Hutchings, Science 321 (2008) 1331.
[13] C. Harding, V. Habibpour, S. Kunz, A.N.S. Farnbacher, U. Heiz, B. Yoon, U. Landman, J. Am. Chem. Soc. 131 (2009) 538.
[14] D. Widmann, R.J. Behm, Angew. Chem. Int. Ed., in press. doi:10.1002/anie.201102062.
[15] Th. Risse, Sh. Shaikhutdinov, N. Nilius, M. Sterrer, H.J. Freund, Acc. Chem. Res. 41 (2008) 949.
[16] D. Astruc (Ed.), Nanoparticles and Catalysis, Wiley-VCH, Weinheim, 2008.
[17] A.S.K. Hashmi, G.J. Hutchings, Angew. Chem. Int. Ed. 45 (2006) 7896.
[18] A. Corma, H. Garcia, Chem. Soc. Rev. 37 (2008) 2096.
[19] J.E. Bailie, G.J. Hutchings, Chem. Commun. (1999) 2151.
[20] R. Zanella, C. Louis, S. Giorgio, R. Touroude, J. Catal. 223 (2004) 328.
[21] P. Claus, Appl. Catal. A 291 (2005) 222.
[22] A. Corma, P. Serna, Science 313 (2006) 332.
[23] M. Boronat, P. Concepción, A. Corma, S. González, F. Illas, P. Serna, J. Am. Chem. Soc. 129 (2007) 16230.
[24] F. Bocuzzi, A. Chiorino, M. Manzoli, D. Andreeva, T. Tabakova, L. Ilieva, V. Iadakiev, Catal. Today 75 (2002) 169.
[25] Q. Fu, H. Saltsburg, M. Flytzani-Stephanopoulos, Science 301 (2003) 935.
[26] J. Rodriguez, Catal. Today 160 (2011) 3.
[27] H. Tsunoyama, H. Sakurai, N. Ichikuni, Y. Negishi, T. Tsukuda, Langmuir 20 (2004) 11293.
[28] S. Carrettin, J. Guzman, A. Corma, Angew. Chem. Int. Ed. 15 (2005) 2242.
[29] C. Gonzalez-Arellano, A. Abad, A. Corma, H. Garcia, M. Iglesias, F. Sanchez, Angew. Chem. Int. Ed. 46 (2007) 1536.
[30] S.K. Beaumont, G. Kyriakou, R.M. Lambert, J. Am. Chem. Soc. 132 (2010) 12246.
[31] G. Kyriakou, S.K. Beaumont, S.M. Humphrey, C. Antonetti, R.M. Lambert, ChemCatChem 2 (2010) 1444.
[32] A. Primo, F. Quignard, Chem. Commun. 46 (2010) 5593.
[33] A. Corma, R. Juárez, M. Boronat, F. Sánchez, M. Iglesias, H. Garcia, Chem. Commun. 47 (2011) 1446.
[34] C. Della Pina, E. Falletta, L. Prati, M. Rossi, Chem. Soc. Rev. 37 (2008) 2077.
[35] S. Biella, M. Rossi, Chem. Commun. (2003) 378.
[36] M.D. Hughes, Y.J. Xu, P. Jenkins, P. McMorn, P. Landon, D.I. Enache, A.F. Carley, G.A. Attard, G.J. Hutchings, F. King, E.H. Stitt, P. Johnston, K. Griffin, C.J. Kiely, Nature 437 (2005) 1132.
[37] C. Milone, R. Ingoglia, M. Tropeano, G. Neri, S. Galvagno, Chem. Commun. (2003) 1359.
[38] J. Radnick, C. Mohr, P. Claus, Phys. Chem. Chem. Phys. 5 (2003) 172.
[39] A. Abad, C. Almela, H. García, A. Corma, Chem. Commun. (2006) 3178.

[40] J. Guzman, S. Carrettin, J.C. Fierro-Gonzalez, Y. Hao, B.C. Gates, A. Corma, Angew. Chem. Int. Ed. 44 (2005) 4778.
[41] T. Takei, I. Okuda, K.K. Bando, T. Akita, M. Haruta, Chem. Phys. Lett. 493 (2010) 207.
[42] M. Haruta, Chem. Rec. 3 (2003) 75.
[43] J.A. Rodriguez, L. Feria, T. Jirsak, Y. Takahashi, K. Nakamura, F. Illas, J. Am. Chem. Soc. 132 (2010) 3177.
[44] M. Turner, V.B. Golovko, O.P.H. Vaughan, P. Abdulkin, A. Berenguer-Murcia, M.S. Tikhov, B.F.G. Johnson, R.M. Lambert, Nature 454 (2008) 981.
[45] J. Huang, E. Lima, T. Akita, A. Guzman, C. Qi, T. Takei, M. Haruta, J. Catal. 278 (2011) 8.
[46] T. Ishida, H. Watanabe, T. Bebeko, T. Akita, M. Haruta, Appl. Catal. A: Gen. 337 (2010) 42.
[47] H. Tsunoyama, H. Sakurai, Y. Negishi, T. Tsukuda, J. Am. Chem. Soc. 127 (2005) 9374.
[48] H. Tsunoyama, N. Ichikuni, H. Sakurai, T. Tsukuda, J. Am. Chem. Soc. 131 (2009) 7086.
[49] H. Liu, Y. Liu, Y. li, Zh. Tang, H. Jiang, J. Phys. Chem. C 114 (2010) 13362.
[50] Y. Liu, H. Tsunoyama, T. Akita, S. Xie, T. Tsukuda, ACS Catal. 1 (2011) 2.
[51] A. Vijay, G. Mills, H. Metiu, J. Chem. Phys. 118 (2003) 6536.
[52] A. Roldan, S. Gonzalez, J.M. Ricart, F. Illas, Chem. Phys. Chem. 10 (2009) 348.
[53] M. Boronat, A. Corma, Dalton Trans. 39 (2010) 8538.
[54] L. Alves, B. Ballesteros, M. Boronat, J.R. Cabrero-Antonino, P. Concepción, A. Corma, M.A. Correa-Duarte, E. Mendoza, J. Am. Chem. Soc. 133 (2011) 10251.
[55] J. Gong, C.B. Mullins, Acc. Chem. Res. 42 (2009) 1063.
[56] X. Liu, B. Xu, J. Haubrich, R.J. Madix, C.M. Friend, J. Am. Chem. Soc. 131 (2009) 5757.
[57] H. Shi, C. Stampfl, Phys. Rev. B 76 (2007) 075327.
[58] T.A. Baker, B. Xu, X. Liu, E. Kaxiras, C.M. Friend, J. Phys. Chem. C 113 (2009) 16561.
[59] R.A. Sheldon, I.W.C.E. Aerends, G.J. ten Brink, A. Dijksman, Acc. Chem. Res. 35 (2002) 774.
[60] T. Mallat, A. Baiker, Chem. Rev. 104 (2004) 3027.
[61] A. Abad, P. Concepción, A. Corma, H. García, Angew. Chem. Int. Ed. 44 (2005) 4066.
[62] Y. Guan, E.J.M. Hensen, Appl. Catal. A: Gen. 361 (2009) 49.
[63] M. Boronat, A. Corma, F. Illas, J. Radilla, T. Ródenas, M.J. Sabater, J. Catal. 278 (2011) 50.
[64] B.N. Zope, D.D. Hibbits, M. Neurock, R.J. Davis, Science 330 (2010) 74.
[65] J.P. Dever, K.F. George, W.C. Hoffman, H. Soo, Ethylene oxide, in: Kirk-Othmer: Encyclopedia of Chemical Technology, fourth ed., vol. 9, Wiley, New York, 1995, p. 915.
[66] J.R. Monnier, The selective epoxidation of nonallylic olefins over supported silver catalysts, Stud. Surf. Sci. Catal. 110 (1997) 135.
[67] T.A. Nijhuis, M. Makkee, J.A. Moulijn, B.M. Weckhuysen, Ind. Eng. Chem. Res. 45 (2006) 3447.
[68] S.T. Oyama, Mechanisms in Homogeneous and Heterogeneous Epoxidation Catalysis, Elsevier B.V., Amsterdam, 2008.
[69] A. Dow Tullo, BASF to build propylene oxide, Chem. Eng. News 82 (2004) 15.
[70] B. Chowdhury, J.J. Bravo-Suárez, N. Mimura, J. Lu, K.K. Bando, S. Tsubota, M. Haruta, J. Phys. Chem. B 110 (2006) 22995.
[71] B. Chowdhury, J.J. Bravo-Suárez, M. Daté, S. Tsubota, M. Haruta, Angew. Chem. Int. Ed. 45 (2006) 412.
[72] N. Yap, R.P. Andres, W.N. Delgass, J. Catal. 226 (2004) 156.
[73] B. Taylor, J. Lauterbarch, W.N. Delgass, Catal. Today 123 (2007) 50.
[74] B. Taylor, J. Lauterbach, G.E. Blau, W.N. Delgass, J. Catal. 242 (2006) 142.
[75] J.J. Bravo-Suárez, K.K. Bando, J. Lu, M. Haruta, T. Fujitani, S.T. Oyama, J. Phys. Chem. C 112 (2008) 1115.
[76] H. Huang, T. Akita, J. Faye, T. Fujitani, T. Takei, M. Haruta, Angew. Chem. Int. Ed. 48 (2009) 7862.
[77] R.G. Quiller, X. liu, C.M. Friend, Chem. Asian J. 5 (2010) 78.
[78] S. Linic, M.A. Barteau, J. Catal. 214 (2003) 200; J. Am. Chem. Soc. 125 (2003) 4034.
[79] P. Cristopher, S. Linic, J. Am. Chem. Soc. 130 (2008) 11264.
[80] D. Torres, N. Lopez, F. Illas, R.M. Lambert, Angew. Chem. Int. Ed. 46 (2007) 2055.
[81] A. Roldán, D. Torres, J.M. Ricart, F. Illas, J. Mol. Catal. A: Chem. 306 (2009) 6.
[82] L. Nie, K.K. Xin, W.S. Li, X.P. Zhou, Catal. Commun. 8 (2007) 488.
[83] A. de Meijere, F. Diederich, Metal-Catalyzed Cross-Coupling Reactions, vol. 1–2, Wiley-VCH, Weinheim, 2004.
[84] J. Hassan, M. Sevignon, Ch. Gozzi, E. Schulz, M. Lemaire, Chem. Rev. 102 (2002) 1359.
[85] C. González-Arellano, A. Corma, M. Iglesias, F. Sánchez, Chem. Commun. (2005) 1990.
[86] D. Zhu, S.V. Lindemann, J.K. Kochi, Organometallics 18 (1999) 2241.
[87] S. Carrettin, J. Guzmán, A. Corma, Angew. Chem. Int. Ed. 44 (2005) 2242.